Phase diagram of the iron arsenide superconductors $Ca(Fe_{1-x}Co_x)_2As_2 (0 \leqslant x \leqslant 0.2)$

L. Harnagea,[1,*] S. Singh,[2] G. Friemel,[1] N. Leps,[1] D. Bombor,[1] M. Abdel-Hafiez,[1] A. U. B. Wolter,[1] C. Hess,[1] R. Klingeler,[3] G. Behr,[1] S. Wurmehl,[1] and B. Büchner[1]

[1]*Leibniz-Institute for Solid State and Materials Research, (IFW)-Dresden, D-01171 Dresden, Germany*

[2]*Indian Institute of Science Education and Research (IISER), Pune, Maharashtra 411008, India*

[3]*Kirchhoff Institute for Physics, University of Heidelberg, D-69120 Heidelberg, Germany*

(Received 5 November 2010; published 17 March 2011)

Plateletlike single crystals of the $Ca(Fe_{1-x}Co_x)_2As_2$ series having lateral dimensions up to 15 mm and thicknesses up to 0.5 mm were obtained from the high-temperature solution-growth technique using Sn flux. Upon Co doping, the c axis of the tetragonal unit cell decreases, while the a axis shows a less significant variation. Pristine $CaFe_2As_2$ shows a combined spin-density wave and structural transition near $T = 166$ K, which gradually shifts to lower temperatures and splits with increasing Co doping. Both transitions terminate abruptly at a critical Co concentration of $x_c = 0.075$. For $x \geqslant 0.05$, superconductivity (SC) appears at low temperatures with a maximum transition temperature T_C of around 20 K. The SC volume fraction increases with Co concentration up to $x = 0.09$ followed by a gradual decrease with a further increase of the doping level. The electronic phase diagram of the $Ca(Fe_{1-x}Co_x)_2As_2$ ($0 \leqslant x \leqslant 0.2$) series is constructed from the magnetization and electric resistivity data. We show that the low-temperature SC properties of Co-doped $CaFe_2As_2$ differ considerably from those of $BaFe_2As_2$ reported previously. These differences seem to be related to the extreme pressure sensitivity of $CaFe_2As_2$ relative to its Ba counterpart.

DOI: 10.1103/PhysRevB.83.094523 PACS number(s): 74.70.Xa, 74.25.Bt, 74.25.Dw

I. INTRODUCTION

Iron pnictides have attracted enormous attention since the discovery of superconductivity (SC) in fluorine-doped LaOFeAs with an SC transition temperature (T_C) of 26 K.[1] Shortly after this discovery, higher T_C values were achieved in these oxypnictides, either by replacing La with smaller size rare-earth ions,[2–4] or by applying pressure,[5] elevating T_C in this class of materials to as high as 55 K.[4] These compounds adopt a layered structure consisting of an alternating stack of LaO and FeAs layers perpendicular to the crystallographic c axis. Since the original discovery, several other families of Fe-based layered high T_C SCs have also been discovered.[6–9] One of these families constitutes the $ThCr_2Si_2$ structure-type AFe_2As_2 (122 family of compounds, A = Ca,Sr,Ba,Eu) intermetallics. They adopt a layered structure analogous to oxypnictides with LaO layers replaced by layers of A. The pristine compounds are characterized as poor metals showing structural transitions in the temperature range of 140–205 K,[10–14] and an antiferromagnetic (AFM) ground state due to spin-density wave (SDW) formation of the Fe 3d spins. Analogous to the oxypnictides, SC can be induced in these compounds, with T_C as high as 38 K, either by chemical substitution (electron-hole doping) or by external pressure.[6,15–22] The electronic phase diagrams for Co-doped Ba122 and Sr122 compounds were reported based on single-crystalline studies.[23–26] In the Co-doped Ba122 series, the electronic phase diagrams reported by several groups showed good agreement with each other,[23–25] which is an indication that reproducible single crystals of these compounds can be grown for comprehensive investigations. More recently, SC has also been reported in 4d and 5d transition-metal-doped Ba122 (Ref. 19) and Sr122 compounds,[20] and their phase diagrams have also been mapped out. While the electron and hole doped $BaFe_2As_2$ and $SrFe_2As_2$ series of compounds have remained very much in focus, studies on the analogous $CaFe_2As_2$ compounds are very scarce.

Recently, pristine $CaFe_2As_2$ has attracted a great deal of attention due to the extreme sensitivity of its structural and magnetic behavior to external pressure. Upon application of a modest hydrostatic pressure of 0.35 GPa, the first-order transition from the tetragonal (T) paramagnetic state to the orthorhombic (O) AFM one is suppressed, and above 0.35 GPa, it completely vanishes, being replaced by a first-order transition to a low-temperature-collapsed tetragonal (cT) nonmagnetic phase. Further application of pressure leads to an increase of the transition temperature from the T to the cT phase crossing room temperature around 1.7 GPa.[21,27,28]

It is noteworthy that this behavior crucially depends on the hydrostaticity of the pressure medium. In He-gas cells where hydrostatic conditions can be closely realized, first-order-like phase transitions were observed, and at low temperatures, the sample exhibits single-crystallographic and magnetic phases.[29]

In contrast, the transition broadens, and the sample enters into a low-temperature multicrystallographic phase when liquid-media cells are used.[28] Interestingly, SC at low temperatures is observed only for the later case, indicating that the nonhydrostaticity of the pressure medium is an important ingredient in stabilizing a SC state in $CaFe_2As_2$ under pressure.[21]

The SC phase is characterized by a dome ($T_C \sim 12$ K) centered at 0.5 GPa, extending from 0.23 up to 0.86 GPa.[21] These findings were further reinforced in Ref. 30 where SC below 10 K was reported under uniaxial pressure.

Recently, it was shown that electronic doping through substituting of Fe for Co in $CaFe_2As_2$ also leads to the appearance of SC at temperatures below about 20 K.

More specifically, about 3% Co doping in Ca122[31] (4% in Ref. 32) results in complete suppression of the magnetic/structural transition and emergence of SC below 17 K (20.4 K in Ref. 32).

However, a systematic study aimed at understanding the influence of progressive increase in the cobalt-doping level in Ca122 is still lacking. The extreme sensitivity of $CaFe_2As_2$ on applied pressure suggests that, in addition to changing the electronic-doping level, the effect of chemical pressure upon Co substitution might be relevant too. Hence, one should expect a more complex influence of Co doping on Ca122 than in the other members of the 122 family, which motivated us to take up the present studies.

Here, we present a complete doping dependence of magnetic, structural, and SC properties of single-crystalline $Ca(Fe_{1-x}Co_x)_2As_2$ samples over a wide doping range from $x = 0$ to $x = 0.20$.

Experimental procedures and single-crystal-growth experiments are presented in Sec. II. Single crystals were characterized using different techniques that are presented and are discussed in Sec. III. Finally, the resulting phase diagram of $Ca(Fe_{1-x}Co_x)_2As_2$ is shown and is compared with the well-studied case of $Ba(Fe_{1-x}Co_x)_2As_2$, which allowed us to make some general preliminary remarks regarding the role of electron doping vis-à-vis to chemical pressure due to Co doping in the 122 family.

II. EXPERIMENTAL PROCEDURE

Single crystals of $Ca(Fe_{1-x}Co_x)_2As_2$ ($0 \leqslant x \leqslant 0.20$) were grown by employing the high-temperature solution-growth method with Sn flux. All room-temperature processing (weighing, mixing, grinding, and storage) was carried out in an Ar-filled glove box (O_2 and moisture level less than 0.1 ppm). The growth experiments were carried out in three steps. In the first step, the precursor materials (CaAs, Fe_2As, and Co_2As) were prepared by reacting stoichiometric quantities of the constituents under vacuum at temperatures less than 900 °C. Fe_2As and Co_2As are prepared by mixing Fe (Alfa Aesar, 99.998%) and Co (Heraeus, 99.8%) powders, respectively, with a stoichiometric amount of arsenic lumps (Alfa Aesar, 99.999%) after removing the surface oxidation products by the sublimation method. For synthesis of CaAs, Ca shots (Merck, 98.5%, 2–6-mm shots) and As lumps were physically separated in a quartz ampoule sealed under vacuum, slowly heated up to 850 °C. This temperature was maintained for a period of 2 days allowing As vapors to slowly react with Ca to form CaAs. In the second step, stoichiometric quantities of the prereacted materials CaAs, Co_2As, and Fe_2As were weighed, were grounded, were pressed into pellets, and were sealed in a quartz ampoule under vacuum. The ampoule was slowly heated to 750 °C, kept there for 10 h, and then further heated to 850 °C for another 15 h before cooling to room temperature. In the final step, the sintered $Ca(Fe_{1-x}Co_x)_2As_2$ pellets and the Sn shots, taken in a molar ratio of 1:30, were placed in an alumina crucible together with a second catch crucible containing quartz wool and were subsequently sealed in a quartz ampoule under vacuum. The charge was slowly heated to 1090 °C, kept there for 24 h to ensure the homogenization, and then cooled down to 600 °C under a slow cooling rate of 2.5 °C per hour. At this temperature, the Sn flux was decanted by flipping the ampoule upside down. After 3 to 4 h of waiting, the ampoule was cooled down to room temperature by switching off the furnace. We found that the three-step procedure described above prevents the growth of a competing orthorhombic phase of stoichiometry $CaFe_4As_3$ that can easily be identified due to its thin needlelike morphology contrary to the plateletlike single crystals of the $CaFe_2As_2$ phase. The formation of this parasitic phase also has been recognized and has been reported earlier by other groups.[10,33] However, using our protocol, only plateletlike crystals of $CaFe_2As_2$ can be obtained. In Figs. 1(a) and 1(b), two representative pictures of as-grown single crystals on a millimeter-size grid are shown. All crystals are plateletlike, shiny, malleable, and prone to exfoliation. Their lateral dimensions are as large as 15 mm and thickness ranges from 200 to 500 μm.

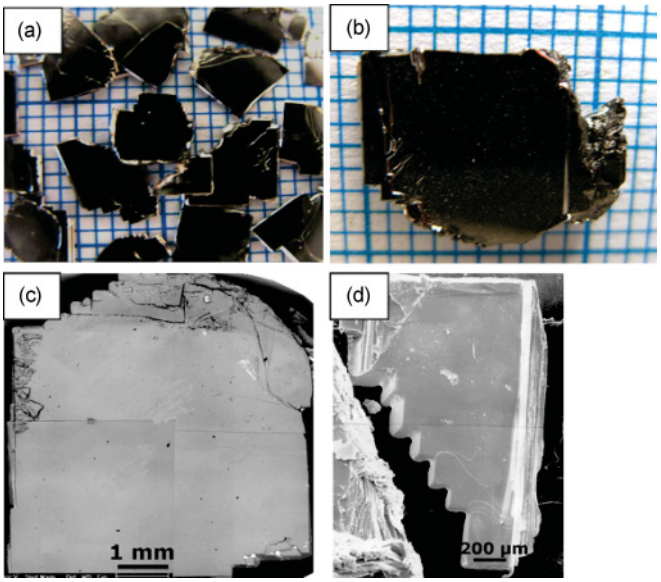

FIG. 1. (Color online) (a),(b) Typical flux-grown single crystals of $Ca(Fe_{1-x}Co_x)_2As_2$ ($x_N = 0.05, 0.15$). The grid in each crystal is millimeter size. (c),(d) Two representative SEM images of as-grown single crystals of $Ca(Fe_{1-x}Co_x)_2As_2$ (see text for details).

The lattice parameters of all of the grown crystals were determined by x-ray powder diffraction (using a Rigaku Miniflex diffractometer [Cu Kα radiation)]. For this purpose, few small single-crystalline pieces from each batch were ground into a fine powder along with high-purity silicon powder added as an internal standard. The growth behavior, crystal morphology, and Co composition were accessed using a scanning electron microscope [(SEM) Philips XL 30] equipped for an energy-dispersive x-ray (EDX) spectroscopy probe and a wavelength dispersive x-ray (WDX) probe. The temperature dependence of the electric resistivity from 4 to 296 K was measured using a standard four-probe technique after cutting a plateletlike crystal in a rectangular parallelepiped shape whose largest surface is parallel to the crystallographic *ab* plane. Current and voltage probes were made using copper wires glued to the sample surface (parallel to the *ab* plane) using silver epoxy. The magnetization measurements were performed using a superconducting quantum interference device magnetometer (MPMS-XL5) from Quantum Design. Data have been obtained in the temperature range of 2–50 K in a magnetic field of 2 mT and between 2 and 350 K in an applied magnetic field of 1 T.

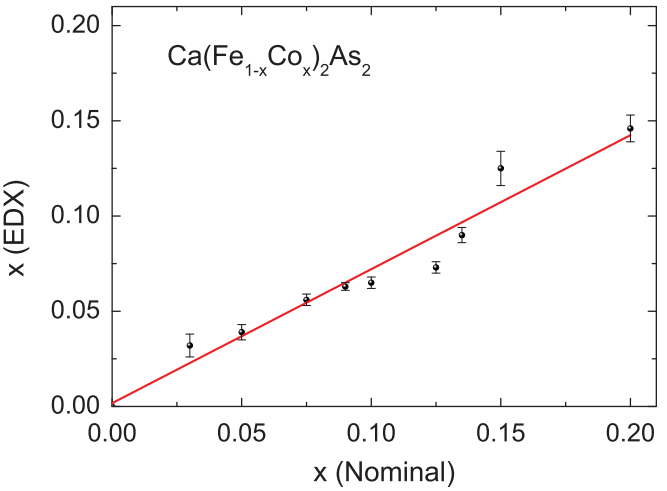

FIG. 2. (Color online) Co composition determined by means of EDX of $Ca(Fe_{1-x}Co_x)_2As_2$ single crystals as a function of nominal concentration x. The dashed line is a linear fit to the data with a slope of 0.7 (see text for details).

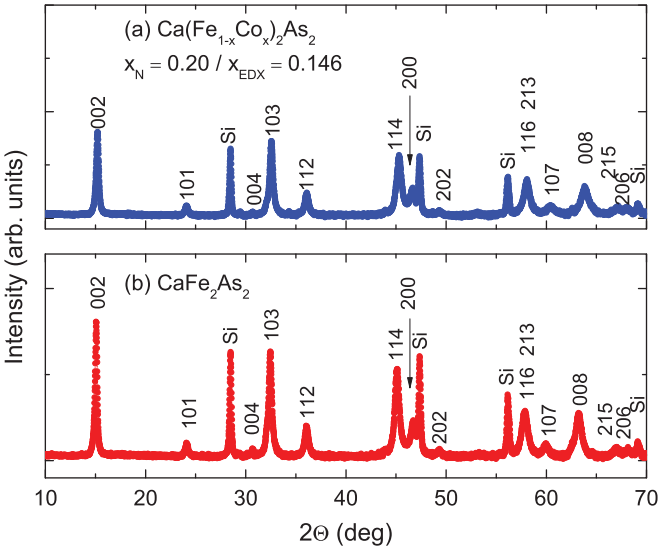

FIG. 3. (Color online) Powder x-ray diffraction pattern of $Ca(Fe_{1-x}Co_x)_2As_2$ ($x_N = 0,0.20$) single crystals. Peaks marked Si are due to silicon added as an internal standard.

III. RESULTS AND DISCUSSIONS

A. Structure analysis, composition, and the growth behavior of $Ca(Fe_{1-x}Co_x)_2As_2$ single crystals

Several plateletlike single crystals from each growth experiment were examined in detail under a SEM equipped with EDX and WDX probes. On each sample, the composition is determined using the EDX data averaged over 16–25 different spots. The EDX data plotted in Fig. 2 show that the actual Co content of these crystals is generally smaller than the nominal value. We observed that the standard deviation in Co concentration measured over several samples of the same batch and about 16–25 different spots on each sample is less than 0.3 at.%, which is within the error limit of the EDX technique (1 to 2 at.%). These results demonstrate a fairly homogeneous distribution of Co within a single crystal and several single crystals of the same batch. Henceforth, since the precision of EDX is limited, we will refer to our single crystals by their nominal Co composition (x_N), quoting their EDX value (x_{EDX}) wherever needed. A linear fit (dashed line in Fig. 2) of EDX compositions as a function of nominal Co concentrations exhibits a slope of about 0.7, which allows converting nominal values into EDX values and vice versa.

Here, it should be mentioned that, in the case of $BaFe_2As_2$ single crystals grown using Sn flux, the presence of up to 1 at.% of Sn incorporation in the structure has been reported.[15,34] In order to exclude the incorporation of Sn in our crystals, we carried out WDX analysis at several points on the single crystals and repeated this experiment for several pieces from different batches. However, no trace of Sn in our single crystals could be detected using WDX analysis. Moreover, the resistivity and magnetization data of our undoped single crystals agree with those reported in the literature for both Sn and self-flux-grown single crystals,[16,33] unlike the case of Ba122, where the behavior of Sn-grown crystals markedly differ from those of self-flux-grown and polycrystalline samples.[11,17,34] Therefore, we can exclude any Sn incorporation in our single crystals. The difference in growth behavior between Ba122 and Ca122 could be related to the smaller ionic size of Ca compared to that of Ba.

Figure 3 shows representative powder-diffraction patterns of the end members $Ca(Fe_{1-x}Co_x)_2As_2$ ($x_N = 0,0.20$). The observed powder pattern is indexed based on $ThCr_2Si_2$-type tetragonal structure (space group: *I4/mmm*, No. 139). Generally, the samples proved to be single phase, only arbitrarily did we observe the diffraction lines of Sn due to the residual flux sticking on the surface of the single crystals. The lattice parameters of the parent compound obtained from the powder pattern are $a_0 = 3.883$ Å and $c_0 = 11.750$ Å. These values are in good agreement with those previously reported in the literature.[16,35] The estimate error in the lattice parameters is about 0.001–0.002 Å. Figure 4 shows the lattice parameter variation of the Co-doping series as a function of

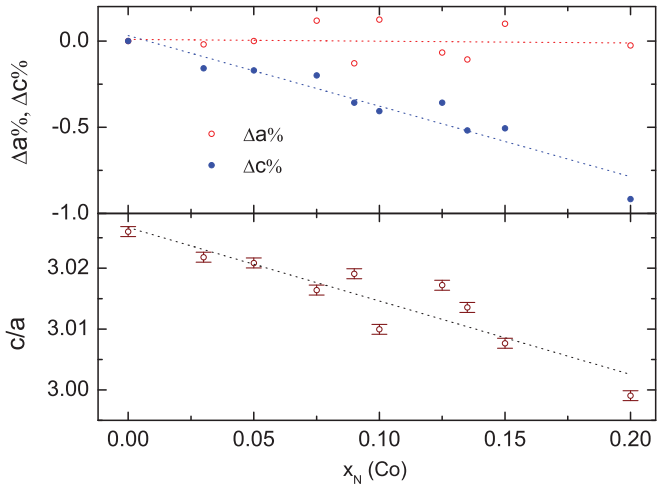

FIG. 4. (Color online) Variation of the lattice parameters as a function of nominal Co content. The lines are guides to the eye. The error bars for $\Delta a\%$ and $\Delta c\%$ are around 10^{-4} Å, smaller than the size of the data point.

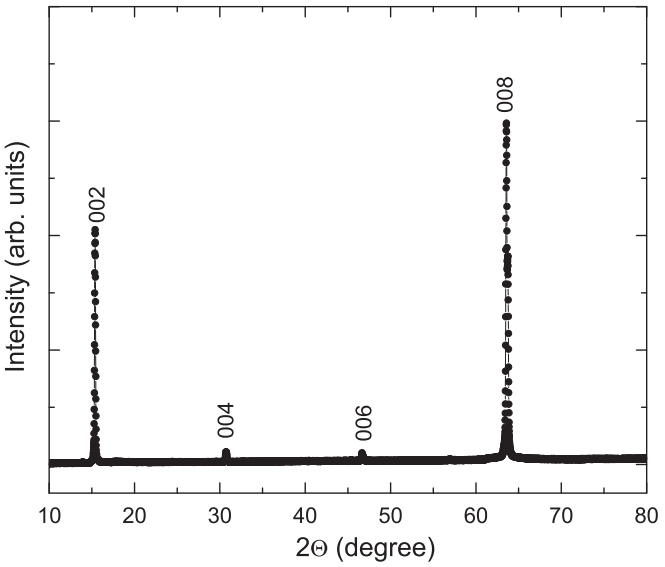

FIG. 5. X-raydiffraction pattern due to a single-crystalline $CaFe_2As_2$ in Bragg-Brentano geometry showing only [0,0,2*l*] reflections (see text for details).

increasing Co content. While the *c* parameter of the tetragonal unit cell decreases upon Co doping, the area of the *ab* plane shows only a slight decrease. The general trend in the variation of the cell parameters in $Ca(Fe_{1-x}Co_x)_2As_2$ is quite similar to that observed in the Co-doped Ba122 series of compounds.[25] However, the changes in the *c* axis, upon Co doping, are more pronounced in the Ca122 than in the Ba122 series. Additionally, an x-ray diffraction experiment was also performed by mounting a single-crystalline platelet in Bragg-Brentano geometry. In this case, the diffraction pattern showed only peaks with Miller indices [0,0,2*l*] ($l = 1,2,3,\ldots$), which implies that the *c* axis is perpendicular to the plane of the platelet (Fig. 5).

We have investigated the $Ca(Fe_{1-x}Co_x)_2As_2$ single-crystal habits, morphology, and growth behavior by electron microscopy. Few selected SEM images of $Ca(Fe_{1-x}Co_x)_2As_2$ single crystals are shown in Fig. 1. These crystals grow as a layered structure, exhibit a plateletlike morphology, and are easy to cleave along the *ab* plane. The crystals are malleable, and the layers present a high tendency to exfoliate as shown in Figs. 1(a) and 1(b). Figure 1(b) shows that the crystals present macrosteps (or microsteps) in the plane of the platelet, indicating a layer-by-layer growth mechanism due to step propagation. Occasionally, we observed the presence of step bunches on the plane of the platelets (not shown). Here, the growth seems to be hindered due to surface Sn inclusions. In the same way, Sn precipitates can be trapped as inclusions (not shown).

B. Normal- and SC-state properties

The temperature dependence of the in-plane resistivity $\rho(T)$ of $Ca(Fe_{1-x}Co_x)_2As_2$ single crystals is shown in Fig. 6. The data for each sample are normalized for the value of resistivity at $T = 296$ K. The resistivity data for the pristine $CaFe_2As_2$ compound exhibits a metallic behavior over the entire temperature range with a prominent first-

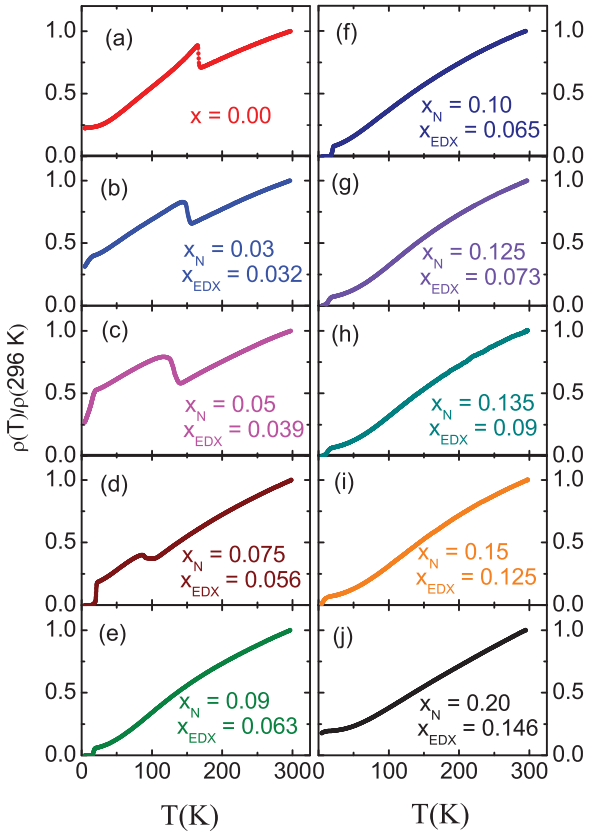

FIG. 6. (Color online) Temperature dependence of the in-plane electrical resistivity of $Ca(Fe_{1-x}Co_x)_2As_2$ single crystals, normalized to the resistivity value at 296 K. x_N and x_{EDX} are nominal and EDX composition, respectively.

order anomaly at $T_0 \sim 166$ K, where the resistivity shows a steplike increase upon cooling [Figs. 6(a)–7(a)]. The position and shape of the anomaly is in agreement with the data previously reported. We should note that the temperature, where the anomaly is observed, can range between 165 and 172 K,[10,16,35] depending on the growth method. Upon cooling below T_0, the crystal symmetry lowers from tetragonal to orthorhombic; concomitantly, the Fe moments order AFM.[10,36] The temperature variation of resistivity also shows a hysteresis of about 2 K between the cooling and the warming runs at the combined structural/magnetic transition (not shown) consistent with previous transport studies.[10,32]

Upon Co substitution, the sharp first-order structural/magnetic anomaly of the parent compound gradually broadens and shifts to lower temperatures [Figs. 6(a)–6(d) and Figs. 7(a)–7(d)], andit is completely suppressed for Co concentrations larger than 0.075. Figure 7 shows the splitting of the structural and magnetic transitions for the intermediate values of Co concentration. We mention that our thermal expansion data on $Ca(Fe_{0.925}Co_{0.075})_2As_2$ clearly confirm the presence of two distinct transitions.[37]

We assigned the first transition to the strong change in the slope of $d\rho/dT$, while the second transition was defined as the inflection point of the $d\rho/dT$ curve in line with Ref. 25 as demonstrated in Fig. 7.

The first derivative of resistivity ($d\rho/dT$), for $x_N = 0.03$, shows no distinct difference between the structural and the

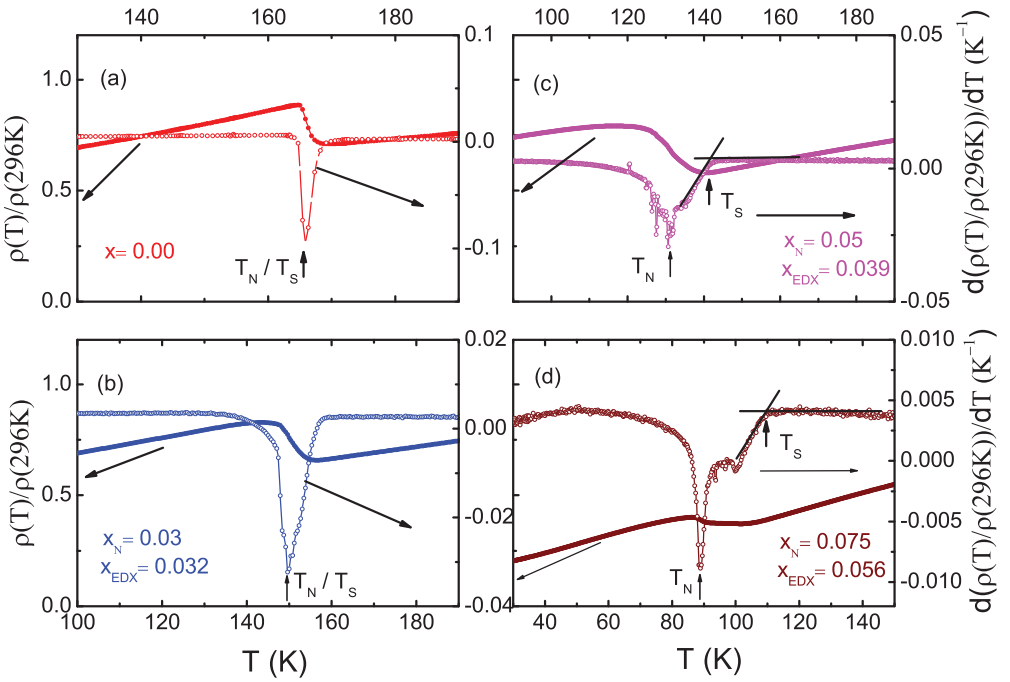

FIG. 7. (Color online) Normalized resistivity $\rho(T)/\rho$ (296 K) of $Ca(Fe_{1-x}Co_x)_2As_2$ ($x_N = 0.00, 0.03, 0.05, 0.075$) and its first derivate plotted as of the temperature. The arrows are indicating the magnetic (T_N) and the structural transition (T_S).

magnetic transitions [Fig. 7(b)]. However, the temperature interval of the transition is broader compared to the undoped sample and is shifted by about 17 K to lower temperatures with respect to the parent compound. For $x_N = 0.05$ and 0.075, the combined structural/magnetic anomaly of the pristine compound actually splits into two distinct anomalies at 142, 131 and 109, 89 K, for $x_N = 0.05$ and 0.075, respectively [Figs. 7(c) and 7(d)]. The error in the determination of the structural (T_S) and magnetic (T_N) transition temperatures can be estimated at around 3 K if we take into account that the peak in the first derivate of the resistivity is relatively broad [Figs. 7(b)–7(d)]. Based on a recent neutron study in analogous Ba122 compounds,[38] we have tentatively attributed the lower temperature to the onset of antiferromagnetic order and the higher temperature to the occurrence of the structural phase transition. Neutron studies on Co-doped Ca122 samples would be helpful in addressing this point further in the case of the Ca series.

In the following, we will discuss the resistivity behavior of the samples, which presents a partial or complete drop to zero resistivity at low temperatures as shown in Fig. 8 where the normalized resistivity, $\rho(T)/\rho$ (30 K), is shown below $T = 30$ K. Interestingly, the sample with the lowest Co concentration in our studies ($x_N = 0.03$) already shows a slight decrease in the resistivity at low temperatures, which can be associated with the onset of spurious SC below about 15 K.

With increasing Co concentration, the SC drop gets more pronounced and shifts to higher temperatures, however, the resistivity remains finite down to $T = 4$ K at $x_N = 0.05$.

In contrast, zero resistivity at low temperatures is observed for Co concentrations above and including 0.075 and up to 0.135. T_C from the resistivity curve, T_C^ρ (determined using the 90% criterion; i.e., the temperature where resistivity has decreased by 90% of its normal-state value), is estimated to be 18.3, 15.5, 17.6, 8, and 7.9 K for $x_N = 0.075, 0.09, 0.10, 0.125, 0.135$. For higher Co concentration, T_C decreases further, and the SC drop turns partial as for the underdoped samples. Thus, at first sight, the evolution of SC and the suppression of the high-temperature structural/magnetic transition in $Ca(Fe_{1-x}Co_x)_2As_2$ seems to follow a trend analogous to the $Ba(Fe_{1-x}Co_x)_2As_2$ compounds. However, in the present case, T_C attains its maximum value ($x_N = 0.075$) when the structural/magnetic anomaly is still present at relatively high temperatures close to $T = 100$ K, and upon further increase of the Co concentration, the structural/magnetic

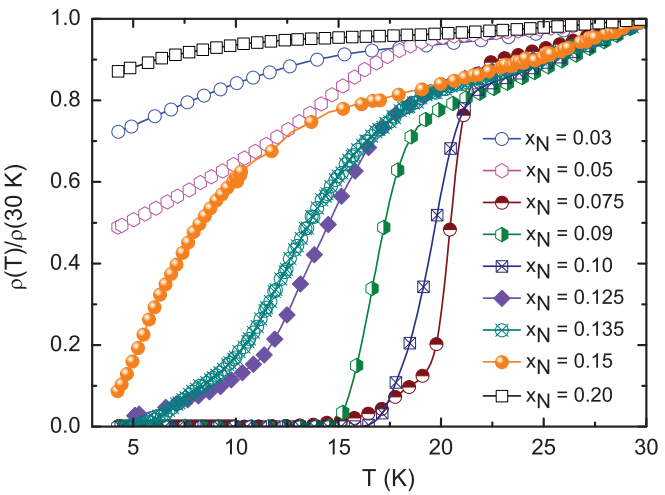

FIG. 8. (Color online) Low-temperature resistivity $\rho(T)/\rho$ (30 K) of $Ca(Fe_{1-x}Co_x)_2As_2$ showing the evolution of the SC transition with Co concentration.

anomaly vanishes abruptly, while T_C changes only marginally. The SC transition width (ΔT_C^ρ) for these single crystals is estimated using: $\Delta T_C^\rho = [T\,(90\%)–T\,(10\%)]$, where T (90%) and T (10%), respectively, are the temperatures where $\rho(T)$ is 90% and 10% of its normal-state value. The value of ΔT_C^ρ is around 3 K for x_N between 0.075 and 0.10 and is higher than 5 K for $x_N = 0.125, 0.135$. These transition widths are very large compared to the analogous Ba compounds. For example, ΔT_C^ρ for an optimally Co-doped Ba122 sample is about 0.7 K.[17,39] We will inquire into these differences in detail later after having presented the other salient features of our resistivity and magnetization data. However, here, it should be remarked that these samples exhibit a fairly homogeneous Co distribution within the limits of the EDX analysis as discussed in Sec. II.

We briefly remark on the residual resistivity ratio (RRR) of the $Ca(Fe_{1-x}Co_x)_2As_2$ series taken as RRR = ρ(296 K)/ρ(25 K). The parent compound has a resistivity of ~3.7 $\mu\Omega$m at 296 K, and it presents a RRR of about 4, which is in good agreement with the data previously reported.[16,31] For the samples with less than 5% Co content, the RRR is ~2 and increases with further increase in the doping level up to 18.2 at 10% Co content, which is then followed by a decrease to 9.7 at $x_N = 0.2$. The high RRR values are usually interpreted as a signature of the high quality of a single crystal. However, we should note that, in the case of these SDW ordering compounds, where parts of the Fermi surface are gapped in the SDW state, it is uncertain to conclude a higher crystalline quality from a large RRR value. The actual value of the resistivity at low temperatures in such cases is determined by a delicate balance between a reduced carrier density (caused by the gap) and an enhanced carrier mean free path (due to reduced scattering at low temperatures) both of which depend differently on the sample purity.

Now, we turn to the magnetic properties of our samples. Figure 9 shows the temperature dependence of M/H of $Ca(Fe_{1-x}Co_x)_2As_2$ single crystals measured under zero-field-cooled conditions in a magnetic field of 1 T applied along the *ab* plane.[40] The pristine $CaFe_2As_2$ compound exhibits a sharp anomaly at 166 K due to the combined structural/magnetic transition consistent with the resistivity data discussed above. The overall behavior of magnetization in the pristine compound is similar to that reported previously.[35] The increase in magnetization at temperatures below 25 K is reminiscent of a Curie-like tail due to magnetic impurities, which is often observed in compounds with small netmagnetization in their antiferromagnetic ground state as in the present case. The magnetization data of the Co-doped samples correlate nicely with their resistivity data shown in Fig. 6. With increasing Co concentration, the anomaly associated with the structural/magnetic phase transition gradually shifts to lower temperatures and disappears completely, and rather abruptly, for $x_N \geqslant 0.075$. The first derivatives of the magnetization curves corresponding to $x_N = 0.05$ and $x_N = 0.075$ show splitting of the structural/magnetic anomaly into two distinct anomalies at $T_S \sim 141$ K, $T_N \sim 131$ K and $T_S \sim 108$ K, $T_N \sim 92$ K, respectively, which is in fair agreement with the analysis of the resistivity data.

The drop in the M/H data of Co-doped samples at low temperatures (Fig. 9) is due to the onset of SC, which is also studied by measurements of the zero-field-cooled volume susceptibility (χ_v) under an applied field of 20 Oe parallel to the *ab* plane of the crystal (Fig. 10). Since the full diamagnetic screening corresponds to $4\pi\chi_v = -1$, the magnitude of the diamagnetic susceptibility, $4\pi\chi_v$, represents the SC volume fraction of the sample. As can be seen in the figure, the SC volume fraction significantly varies with doping concentration.

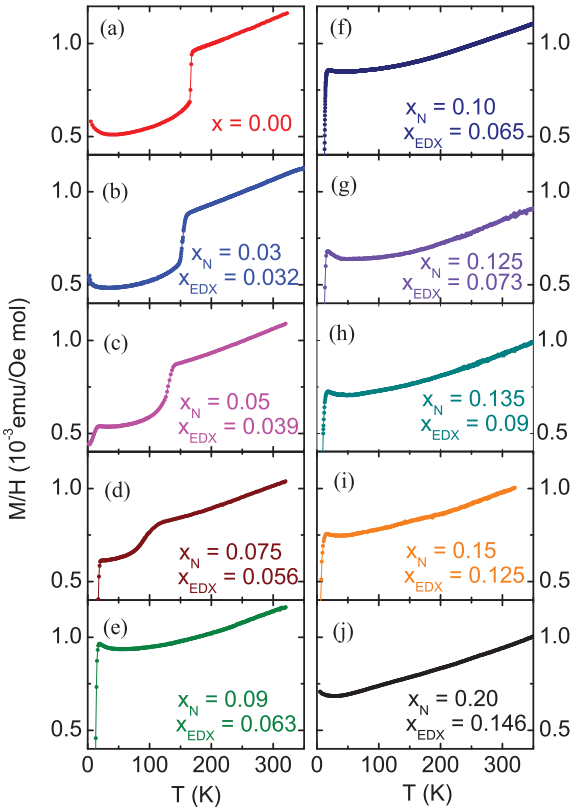

FIG. 9. (Color online) Temperature dependence of the magnetization of $Ca(Fe_{1-x}Co_x)_2As_2$ measured under an applied field of 1 T parallel to the crystallographic basal plane in zero-field conditions.

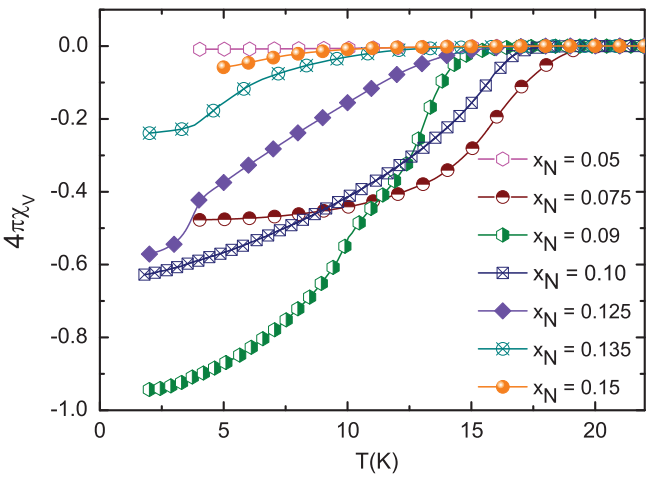

FIG. 10. (Color online) Low-temperature volume magnetic susceptibility of $Ca(Fe_{1-x}Co_x)_2As_2$ single crystals under 20-Oe zero-field-cooled conditions parallel to the crystallographic basal plane.

This variation (Fig. 10) demonstrates that the SC is complete only within a very narrow range of the Co concentration. Interestingly, the sample for which T_C is maximum ($x_N = 0.075$) exhibits only a partial SC volume fraction. The SC transition temperature from the susceptibility plot (T_C^χ) is taken at the intersection point of the slopes extrapolated from the normal state and the SC transition region, respectively. Using this procedure yields T_C of 18.5, 15, 17, 14.1, 11.8, and 11.4 K for samples with $x_N = 0.075, 0.09, 0.10, 0.125, 0.135, 0.15$.

Using this criterion for determining T_C, we observed good agreement between the transition temperature values determined from resistivity and magnetization data for Co doping up to 0.10. On the other hand, a large difference up to 6 K in the values of the transition temperature determined from resistivity and magnetization curves for the samples from the overdoped regime was observed.

However, if we use the onset criterion for extracting the transition temperature from the resistivity data, a fair agreement is observed between T_C values. Note as well that, in contrast, applying an onset criterion for extracting the transition temperature from magnetization data yields only a weak doping-dependent T_C value of around 20 K for all doping levels.

C. Phase diagram

Using the magnetic and the electrical resistivity data, we traced the evolution of the structural/magnetic phase transition and the SC phase transition of $Ca(Fe_{1-x}Co_x)_2As_2$ single crystals as a function of Co content (Fig. 11). In the underdoped side of the phase diagram ($0.05 \leqslant x_N \leqslant 0.075$), there is a small region that shows the apparent coexistence of the orthorhombic/antiferromagnetic phases with SC. This coexistence is particularly remarkable for the sample with $x_N = 0.075$ for which the T_C is maximum, and yet the structural/magnetic anomalies occur at relatively high temperatures close to 100 K. Upon further increasing of the Co concentration, the anomaly is no longer visible in the magnetic and resistivity data, while SC remains, albeit at slightly lower temperatures. Concomitantly, the SC volume fraction increases to full diamagnetic screening at $x_N = 0.09$ (Fig. 12). At $x_N \geqslant 0.10$, both T_C and the SC volume fraction decrease again.

Although the SC region has a usual domelike appearance, the dome maximum appears at the underdoped side of the phase diagram in contrast to the $Ba(Fe_{1-x}Co_x)_2As_2$ phase diagram[25] where the dome maximum appears at optimal doping. In addition, suppression of the structural/antiferromagnetic phase transitions upon Co doping is quite different in Ba and Ca compounds too. In $Ba(Fe_{1-x}Co_x)_2As_2$, the structural/antiferromagnetic transitions are monotonically and continuously suppressed with increasing Co substitution at an initial rate of roughly 15 K per atomic percent Co and disappear above approximately 5.8% Co substitution. In the case of $Ca(Fe_{1-x}Co_x)_2As_2$, on the other hand, the structural/magnetic anomalies are suppressed initially at a rate of approximately 10 K per atomic percent Co but eventually vanish abruptly above $x_N = 0.075$. Nonetheless, similar to the case of Co-doped Ba122, in $Ca(Fe_{1-x}Co_x)_2As_2$, the underdoped region exhibits a splitting of the structural and magnetic phase transitions.

In Fig. 12, we present in detail (a) the variation of the SC transitions temperatures as determined from susceptibility and resistivity data, (b) the SC volume fraction V_{SC}, (c) the transition width ΔT_C, and (d) the residual resistivity ratio as a function of the nominal Co concentration of the samples. The data imply that both the SC volume fraction and the transition width exhibit drastic changes as a function of Co concentration. Interestingly, there is an *inverse* correlation between the transition width and the SC volume fraction. In the range of 7.5%–10% Co content, V_{SC} is increasing, while

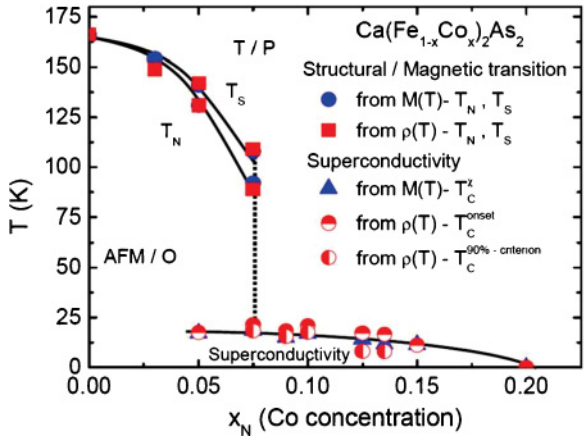

FIG. 11. (Color online) Electronic phase diagram of $Ca(Fe_{1-x}Co_x)_2As_2$ obtained from magnetic and electric resistivity data, showing the suppression of the magnetic/structural phase transitions (blue circles and red squares, T_N, T_S) with increasing Co concentration and the appearance of the SC transition (red half-filled circles, T_C determined from resistivity using the 90% and the onset criteria; blue triangles, T_C determined from magnetization data taken at the intersection point of the slopes extrapolated from the normal state and the SC transition region) with maximum T_C of ~20 K.

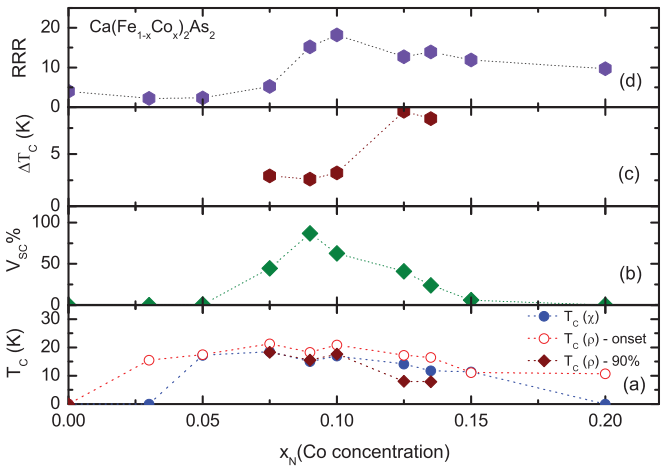

FIG. 12. (Color online) Evolution of SC-state parameters in $Ca(Fe_{1-x}Co_x)_2As_2$ with Co concentration x. (a) SC transition temperatures determined from the susceptibility and the transport data; (b) SC volume fraction determined from the magnetic susceptibility data; (c) variation of the width in the temperature of the resistive SC transition T_C; (d) variation of the residual resistivity ratio with Co concentration. All lines are guides to the eye.

the SC transition is becoming sharper. The data show that the sharpest SC transitions are associated with bulk SC, while the broader transitions are associated with only partial volume SC.[43]

IV. DISCUSSION

In order to understand the salient differences between the physical properties of Ca122 and Ba122, it appears reasonable to invoke chemical pressure effects in addition to pure electronic-doping effects. This can be inferred from the decrease in lattice parameters upon Co doping as shown in Fig. 4. Since Co doping only has a small effect on the crystallographic a axis, the chemical pressure is essentially uniaxial. Such a chemical pressure also appears in the analogous Ba and Sr compounds; however, extreme sensitivity of $CaFe_2As_2$, in particular, to applied uniaxial pressure, complicates the present scenario. Therefore, in Ca122, several competing factors come into play with increasing Co doping. More specifically, Co substitution for Fe not only results in electron doping (prevalent in Ba compounds), but also induces a chemical pressure resulting in competing states at low temperatures that include the orthorhombic (O), the collapsed tetragonal (cT), and the residual untransformed tetragonal phase (T').[30] This conjecture is based on recent uniaxial pressure experiments that stabilized the cT and T' phases at the expense of the orthorhombic phase.[30] Furthermore, it was shown in this paper that pressure-induced SC below $T = 10$ K in pristine $CaFe_2As_2$ arises due to the T' phase stabilized under uniaxial pressure applied along the c axis, while the cT phase does not support SC.

Our data do not allow separating the effects of chemical pressure and electronic doping, but one can qualitatively understand the differences of the Ca122 phase diagram to its Ba and Sr counterparts. In the underdoped region of the phase diagram (i.e., for $x_N = 0.03, 0.05, 0.075$), the onset of SC at a relatively high temperature of about 17 K (compared to the pressure induced T_C of 10 K in pristine $CaFe_2As_2$) most likely arises due to the gradual filling up of the hole pockets due to Co doping, which lowers the antiferromagnetic transition and apparently favors SC analogous to the effect of Co doping in $BaFe_2As_2$. Note, however, that the SC onset is significantly higher in temperature than in Co-doped Ba122.[25] In further contrast to Ba122, upon increasing the Co-doping level, the signatures of the orthorhombic phase and the SDW order disappear abruptly at $x_N \approx 0.075$, which is reminiscent of a similar behavior observed in the fluorine-doped LaOFeAs SCs.[44] For $x_N \leqslant 0.075$, the orthorhombic phase and SC coexist with SDW ordering, such as in Co-doped Ba122 and Sr122. Whether SC coexists with magnetism in the same spatial domains or if there is nanoscopic phase segregation between these phases is a question, however, that needs to be pursued further.

The complete suppression of the T-O transition at $x_N > 0.075$ is accompanied by an enhanced SC volume fraction and a sharpening of ΔT_C (cf. Fig. 12) up to $x_N \sim 0.1$. In analogy with the uniaxial pressures study,[30] one may speculate that the suppressed orthorhombic phase and the enhanced SC properties in this intermediate region of the phase diagram are stabilized by the presence of the T' phase.

In the overdoped region of the phase diagram ($x_N > 0.1$), SC is apparently weakened (Fig. 12). Remarkably, the suppression is significantly more rapid than in the Ba122 case. A plausible scenario to explain this difference is an increasing fraction of the cT phase at low temperatures. In this scenario, upon increasing the Co concentration, the weight fraction of the T' phase decreases in favor of the cT phase as shown in the uniaxial pressure study.[30] This conjecture is corroborated by a rough estimate of the chemical pressure corresponding to a given Co concentration, which can be obtained by comparing the lattice parameters under pressure at $T = 300$ K, given in Ref. 28, to the ambient variation of lattice parameter as a function of Co doping shown in Fig. 4. We find that $x_N = 0.15$ (i.e., for a slightly overdoped compound) translates to an external uniaxial pressure of about 0.5 GPa applied parallel to the c axis. At this uniaxial external pressure, the transition from T to cT phase would appear at around $T = 120$ K (cf. the T-p phase diagram in Ref. 28). Hence, since it is argued that the cT phase does not exhibit SC, the pressure effect, at least qualitatively, implies the presence of a competing phase and, consequently, a more rapid suppression of SC than expected by pure electronic-doping effects. We now discuss the differences in the SC transition width of Co-doped Ca122 samples compared with the analogous Ba compounds. Despite the fact that our $Ca(Fe_{1-x}Co_x)_2As_2$ single crystals appear homogenous within the error bars of EDX analysis and of comparable homogeneity as the analogous Co-doped Ba122 compounds, their SC transition widths are relatively large. Moreover, in the previous study on the Co-doped $CaFe_2As_2$ compound by Kumar *et al.*,[31] the SC transition width reported is as broad as in our samples with similar SC volume fraction. These observations suggest that the broad SC transition in Co-doped Ca122 is an intrinsic property that could be related to the chemical pressure generated upon Co doping, given the extreme pressure sensitivity of Ca122, as discussed earlier. However, the presence of chemical inhomogeneities over nanoscopic length scales in the Ca122 samples cannot be ruled out, which will also lead to a broadening of the SC transition.

V. SUMMARY AND CONCLUSIONS

We have successfully grown large and high-quality single crystals of $Ca(Fe_{1-x}Co_x)_2As_2$ ($0 \leqslant x \leqslant 0.20$) from Sn flux using the high-temperature solution-growth technique. All the grown crystals were found to be phase-pure crystallizing in a tetragonal $ThCr_2Si_2$-type structure. Upon Co doping, the area of the ab plane only slightly varies, while the crystallographic c axis of the tetragonal unit cell decreases at a rate that is even more pronounced than in the case of Co-doped Ba122. A detailed WDX/EDX analysis of these single crystals indicates a fairly homogenous Co distribution with no traces of Sn incorporation in the structure. The actual Co concentration in our samples is found to be smaller than the nominal one ($x_{EDX} \approx 0.7 x_N$). The magnetic and transport data of the parent compound manifest a clear first-order transition (SDW/structural transition) near 166 K, in good agreement with previous reports. Upon doping, the combined SDW/structural transition at 166 K is gradually suppressed and splits into two distinct transitions, giving way to SC with a maximum T_C near 20 K. From the magnetic and

resistivity data, we established the electronic phase diagram of $Ca(Fe_{1-x}Co_x)_2As_2$ ($0 \leqslant x \leqslant 0.20$). Interestingly, the maximum T_C value is observed for 7.5% Co content at which magnetism and SC still coexist. Upon increasing the doping, a small interval with enhanced SC properties in the absence of the orthorhombic/SDW phase is observed up to ∼10% doping level. Further increase of the doping leads to a rather rapid suppression of SC. Our findings suggest that both steric effect due to the chemical pressure as well as electronic doping effects need to be taken into account for understanding the peculiar appearance and disappearance of SC in the Ca122 series of compounds, which differs from their Ba and Sr analogs.

ACKNOWLEDGMENTS

This work was supported by the Deutsche Forschungsgemeinschaft through Grant No. BE1749/12, and the Priority Programme SPP1458 (Grants No. BE1749/13 and No. GR3330/2). We thank M. Deutchmann, S. Müller-Litvanyi, R. Müller, J. Werner, S. Pichl, and S. Gaß for technical support.

*l.harnagea@ifw-dresden.de

[1] Yoichi Kamihara, Takumi Watanabe, Masahiro Hirano, and Hideo Hosono, J. Am. Chem. Soc. **130**, 3296 (2008).
[2] G. F. Chen, Z. Li, D. Wu, G. Li, W. Z. Hu, J. Dong, P. Zheng, J. L. Luo, and N. L. Wang, Phys. Rev. Lett. **100**, 247002 (2008).
[3] Z. A. Ren, J. Yang, W. Lu, W. Yi, G. C. Che, X. L Dong, L. L. Sun, and Z. X. Zhao, Mater. Res. Innovations **12**, 105 (2008).
[4] Ren Zhi-An, Lu Wei, Yang Jie, Yi Wei, Shen Xiao-Li, Li Zheng-Cai, Che Guang-Can, Dong Xiao-Li, Sun Li-Ling, Zhou Fang, and Zhao Zhong-Xian, Chin. Phys. Lett. **25**, 2215 (2008).
[5] Hiroki Takahashi, Kazumi Igawa, Kazunobu Arii, Yoichi Kamihara, Masahiro Hirano, and Hideo Hosono, Nature (London) **453**, 376 (2008).
[6] Marianne Rotter, Marcus Tegel, and Dirk Johrendt, Phys. Rev. Lett. **101**(16), 107006 (2008).
[7] Dinah R. Parker, Michael J. Pitcher, Peter J. Baker, Isabel Franke, Tom Lancaster, Stephen J. Blundell, and Simon J. Clarke, Chem. Commun. 2189 (2009).
[8] Joshua H. Tapp, Zhongjia Tang, Bing Lv, Kalyan Sasmal, Bernd Lorenz, Paul C. W. Chu, and Arnold M. Guloy, Phys. Rev. B **78**, 060505 (2008).
[9] Yoshikazu Mizuguchi, Fumiaki Tomioka, Shunsuke Tsuda, Takahide Yamaguchi, and Yoshihiko Takano, Appl. Phys. Lett. **93**, 152505 (2008).
[10] N. Ni, S. Nandi, A. Kreyssig, A. I. Goldman, E. D. Mun, S. L. Bud'ko, and P. C. Canfield, Phys. Rev. B **78**, 014523 (2008).
[11] Marianne Rotter, Marcus Tegel, Dirk Johrendt, Inga Schellenberg, Wilfried Hermes, and Rainer Pottgen, Phys. Rev. B **78**, 020503(R) (2008).
[12] Jun Zhao, W. Ratcliff II, J. W. Lynn, G. F. Chen, J. L. Luo, N. L. Wang, Jiangping Hu, and Pengcheng Dai, Phys. Rev. B **78**, 140504 (2008).
[13] H. S. Jeevan, Z. Hossain, Deepa Kasinathan, H. Rosner, C. Geibel, and P. Gegenwart, Phys. Rev. B **78,** 052502 (2008).
[14] Q. Huang, Y. Qiu, Wei Bao, M. A. Green, J.W. Lynn, Y. C. Gasparovic, T. Wu, G. Wu, and X. H. Chen, Phys. Rev. Lett. **101**, 257003 (2008).
[15] N. Ni, S. L. Bud'ko, A. Kreyssig, S. Nandi, G. E. Rustan, A. I. Goldman, S. Gupta, J. D. Corbett, A. Kracher, and P. C. Canfield, Phys. Rev. B **78**, 014507 (2008).
[16] G. Wu, H. Chen, T. Wu, Y. L. Xie, Y. J. Yan, R. H. Liu, X. F. Wang, J. J. Yang, and X. H. Chen, J. Phys. Condens. Matter **20**, 422201 (2008).
[17] A. S. Sefat, R. Jin, M. A. McGuire, B. C. Sales, D. J. Singh, and D. Mandrus, Phys. Rev. Lett. **101**, 117004 (2008).
[18] L. J. Li, Y. K. Luo, Q. B. Wang, H. Chen, Z. Ren, Q. Tao, Y. K. Li, X. Lin, M. He, Z. W. Zhu, G. H. Cao, and Z. A. Xu, New J. Phys. **11**, 025008 (2009).
[19] N. Ni, A. Thaler, A. Kracher, J. Q. Yan, S. L. Bud'ko, and P. C. Canfield, Phys. Rev. B **80**, 024511 (2009).
[20] Fei Han, Xiyu Zhu, Peng Cheng, Gang Mu, Ying Jia, Lei Fang, Yonglei Wang, Huiqian Luo, Bin Zeng, Bing Shen, Lei Shan, Cong Ren, and Hai-Hu Wen, Phys. Rev. B **80**, 024506 (2009).
[21] Milton S. Torikachvili, Sergey L. Bud'ko, Ni Ni, and Paul C. Canfield, Phys. Rev. Lett. **101**, 057006 (2008).
[22] Patricia L. Alireza, Y. T. Chris Ko, Jack Gillett, Chiara M. Petrone, Jacqueline M. Cole, Gilbert G. Lonzarich, and Suchitra E. Sebastian, J. Phys.: Condens. Matter **21**, 012208 (2009).
[23] J.-H. Chu, J. G. Analytis, C. Kucharczyk, and I. R. Fisher, Phys. Rev. B **79**, 014506 (2009).
[24] C. Lester, Jiun-Haw Chu, J. G. Analytis, S. C. Capelli, A. S. Erickson, C. L. Condron, M. F. Toney, I. R. Fisher, and S. M. Hayden, Phys. Rev. B **79**, 144523 (2009).
[25] N. Ni, M. E. Tillman, J.-Q. Yan, A. Kracher, S. T. Hannahs, S. L. Bud'ko, and P. C. Canfield, Phys. Rev. B **78**, 214515 (2008).
[26] J. S. Kim, Seunghyun Khim, H. J. Kim, M. J. Eom,1 J. M. Law, R. K. Kremer, Ji Hoon Shim, and Kee Hoon Kim, Phys. Rev. B **82**, 024510 (2010).
[27] A. Kreyssig, M. A. Green, Y. Lee, G. D. Samolyuk, P. Zajdel, J. W. Lynn, S. L. Bud'ko, M. S. Torikachvili, N. Ni, S. Nandi, J. B. Leão, S. J. Poulton, D. N. Argyriou, B. N. Harmon, R. J. McQueeney, P. C. Canfield, and A. I. Goldman, Phys. Rev. B **78**, 184517 (2008).
[28] A. I. Goldman, A. Kreyssig, K. Prokeš, D. K. Pratt, D. N. Argyriou, J. W. Lynn, S. Nandi, S. A. J. Kimber, Y. Chen, Y. B. Lee, G. Samolyuk, J. B. Leão, S. J. Poulton, S. L. Bud'ko, N. Ni, P. C. Canfield, B. N. Harmon, and R. J. McQueeney, Phys. Rev. B **79**, 024513 (2009).
[29] W. Yu, A. A. Aczel, T. J. Williams, S. L. Bud'ko, N. Ni, P. C. Canfield, and G. M. Luke, Phys. Rev. B **79**, 020511 (2009).
[30] K. Prokeš, A. Kreyssig, B. Ouladdiaf, D. K. Pratt, N. Ni, S. L. Bud'ko, P. C. Canfield, R. J. McQueeney, D. N. Argyriou, and A. I. Goldman, Phys. Rev. B **81**, 180506(R) (2010).
[31] Neeraj Kumar, R. Nagalakshmi, R. Kulkarni, P. L. Paulose, A. K. Nigam, S. K. Dhar, and A. Thamizhavel, Phys. Rev. B **79**, 012504 (2009).
[32] Marcin Matusiak, Zbigniew Bukowski, and Janusz Karpinski, Phys. Rev. B **81**, 020510(R) (2010).

[33] N. J. Curro, A. P. Dioguardi, N. ApRoberts-Warren, A. C. Shockley, and P. Klavins, New J. Phys. **11**, 075004 (2009).

[34] G. L. Sun, D. L. Sun, M. Konuma, P. Popovich, A. Boris, J. B. Peng, K.-Y. Choi, P. Lemmens, and C. T. Lin, e-print arXiv:0901.2728v3 (unpublished).

[35] F. Ronning, T. Klimczuk, E. D. Bauer, H. Volz, and J. D. Thompson, J. Phys. Condens. Matter **20**, 322201 (2008).

[36] A. I. Goldman, D. N. Argyriou, B. Ouladdiaf, T. Chatterji, A. Kreyssig, S. Nandi, N. Ni, S. L. Bud'ko, P. C. Canfield, and R. J. McQueeney, Phys. Rev. B **78**, 100506 (2008).

[37] L. Wang, Ph.D. thesis, TU Dresden, 2010.

[38] D. K. Pratt, W. Tian, A. Kreyssig, J. L. Zarestky, S. Nandi, N. Ni, S. L. Bud'ko, P. C. Canfield, A. I. Goldman, and R. J. McQueeney, Phys. Rev. Lett. **103**, 087001 (2009).

[39] S. Aswartham, C. Nacke, G. Friemel, N. Leps, S. Wurmehl, N. Wizent, C. Hess, R. Klingeler, G. Behr, B. Büchner, and S. Singh, J. Cryst. Growth **314**, 341 (2011).

[40] A few of the $Ca(Fe_{1-x}Co_x)_2As_2$ single crystals used in the present paper have also been investigated in Refs. 41 and 42.

[41] R. Klingeler, N. Leps, I. Hellmann, A. Popa, U. Stockert, C. Hess, V. Kataev, H.-J. Grafe, F. Hammerath, G. Lang, S. Wurmehl, G. Behr, L. Harnagea, S. Singh, and B. Büchner, Phys. Rev. B **81**, 024506 (2010).

[42] A. K. Pramanik, L. Harnagea, S. Singh, S. Aswartham, G. Behr, S. Wurmehl, C. Hess, R. Klingeler, and B. Büchner, Phys. Rev. B **82**, 014503 (2010).

[43] We note that, before our measurements of the magnetization in small magnetic fields of 20 Oe, we applied a demagnetization sequence in order to diminish the remanent field. From different demagnetization sequences and after applying the so-called ultra-low-field option, we estimate an error in determining V_{SC} due to the remaining remanent field up to around 10% under our working conditions.

[44] H. Luetkens, H.-H. Klauss, M. Kraken, F. J. Litterst, T. Dellmann, R. Klingeler, C. Hess, R. Khasanov, A. Amato, C. Baines, M. Kosmala, O. J. Schumann, M. Braden, J. Hamann-Borrero, N. Leps, A. Kondrat, G. Behr, J. Werner, and B. Büchner, Nature Mater. **8**, 305 (2009).